JMEPEG (2021) 30:5039–5049
https://doi.org/10.1007/s11665-021-05603-9

1059-9495/$19.00

Small Punch Testing to Estimate the Tensile and Fracture Properties of Additively Manufactured Ti-6Al-4V

Enrico Lucon, Jake T. Benzing, Nicholas Derimow, and Nik Hrabe

Submitted: 21 October 2020 / Revised: 23 December 2020 / Accepted: 18 February 2021 / Published online: 15 March 2021

Small punch (SP) testing is a methodology that uses tiny disks (generally 8 mm in diameter and 0.5 mm thick) to estimate mechanical properties of metallic materials, such as tensile properties, fracture toughness, and ductile-to-brittle transition temperature. Empirical correlations are typically used to infer conventional mechanical properties from characteristic forces and displacements obtained from the test record. The majority of the available literature relates to SP testing of steels, while relatively little is available for other metallic materials. At NIST in Boulder, Colorado, we conducted SP tests on additively manufactured (AM) Ti-6Al-4V with different processing parameters and heat treatment conditions. Force/punch displacement curves appeared different than those typically reported for conventionally manufactured steels, and correlations with tensile and fracture parameters were generally weaker than those published for steel samples. It appears that the application of the SP technique (characterized by a biaxial loading mode) to materials with high anisotropy such as AM materials may be somewhat problematic and therefore of limited applicability.

Keywords additive manufacturing, empirical correlations, fracture toughness, small punch, tensile properties, Ti-6Al-4V

1. Introduction

In the field of experimental techniques based on sub-size or miniaturized specimens, methodologies based on testing tiny disks represent a method for characterizing the mechanical properties of service-exposed plant components or structures with a minimal amount of material extracted from the component and subjected to destructive mechanical testing (Ref 1). Moreover, a significant number of disk specimens can be extracted from mechanical machining leftovers or conventional specimens that were broken during previous tests.

The small punch (SP) test, also known as the disk bend test, was first developed in the mid-1980s (Ref 2, 3) through the use of small TEM size disks (3 mm diameter, 0.25 mm thickness) centrally loaded by a spherical ball or hemispherical punch and expanded into a larger lower die. The test system was a module that could be placed between the loading platens of a tensile machine and subsequently loaded (Ref 3). The outcome is a bulge in the disk rather than a shear cut, as in a similar methodology called the shear punch test (Ref 4). Although

This invited article is part of a special topical focus in the *Journal of Materials Engineering and Performance on Additive Manufacturing*. The issue was organized by Dr. William Frazier, Pilgrim Consulting, LLC; Mr. Rick Russell, NASA; Dr. Yan Lu, NIST; Dr. Brandon D. Ribic, America Makes; and Caroline Vail, NSWC Carderock.

Enrico Lucon, Jake T. Benzing, Nicholas Derimow, and **Nik Hrabe**, Applied Chemicals and Materials Division, National Institute of Standards and Technology (NIST), 325 Broadway, Boulder, CO 80305. Contact e-mail: enrico.lucon@nist.gov.

Abbreviations

AM	Additive manufacturing
ASTM	American Society for Testing and Materials
BSE	Backscattered electrons
CEN	European Committee for Standardization
EBM	Electron beam melting
EDM	Electro discharge machining
HIP	Hot isostatic pressing
ODS	Oxide dispersion strengthening
E_m	In SP testing, total energy calculated up to u_m (J)
E_{PL}	In SP testing, plastic energy calculated up to u_m (J)
E_{SP}	In SP testing, fracture energy calculated up to u_f (J)
ε_f	In SP testing, effective fracture strain
ε_t	In tensile testing, total elongation (%)
ε_u	In tensile testing, uniform elongation (%)
F_e	In SP testing, elastic–plastic transition force (N)
F_{ept}	In SP testing, force at the point of maximum curvature (N)
$F_{e1.5}$	In SP testing, force corresponding to the point where the ratio between area under the curve and above the curve equals 1.5 (N)
$F_{h0/10,off}$	In SP testing, force at the intersection between test record and line parallel to the slope of the initial linear region with an offset of $0.1 \bullet h_0$ (N)
F_{infl}	In SP testing, force at the inflection point of the curve ($d^2F/du^2 = 0$) (N)
F_m	In SP testing, maximum force (N)
$F_{0.1mm,off}$	In SP testing, force at the intersection between the test record and a line parallel to the slope of the initial linear region with an offset of 0.1 mm (N)
$F_{0.48mm}$	In SP testing, force corresponding to a displacement value of 0.48 mm (N)
$F_{0.645mm}$	In SP testing, force corresponding to a displacement value of 0.645 mm (N)

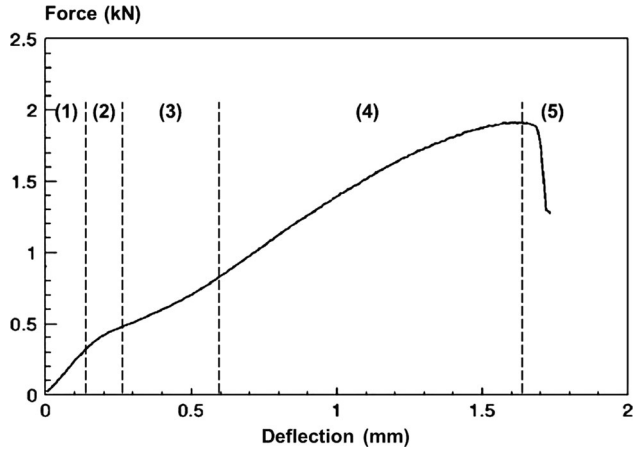

Fig. 1 Typical form of a SP test force–deflection diagram for steel, showing five different regions (Ref 1)

TEM-size disks are still used, nowadays the most popular specimen geometry (which is used in this investigation) is a round disk with a diameter of 8 mm and a thickness of 0.5 mm. The use of square specimens (10 mm × 10 mm) has also been reported (Ref 5).

The general form of a SP force/deflection test record for a steel specimen is shown in Fig. 1 (Ref 1). Five distinct regions can be identified:

1. Elastic region,
2. Departure from linearity,
3. Local bending, transitioning to a membrane stress regime,
4. Membrane stress regime, and
5. Final failure region.

The general form of the test record suggests that yield stress is associated with the change in slope between regions 1 and 2, while the ultimate tensile stress appears related to the maximum force and ductility with maximum deflection. Note that for steels showing low ductility, regions 4 and 5 may be virtually absent or minimized.

Characteristic values of force, displacement, and energy are identified on the test record.* These values are generally fed into empirical relations to obtain estimates of specific mechanical parameters (tensile properties, ductile-to-brittle transition temperature, fracture toughness) for the material under investigation. Numerous empirical correlations can be found in the literature, having been developed by comparing characteristic parameters from SP tests with tensile properties, transition temperature data, and fracture toughness values measured by means of conventional tests.

In most cases, correlations appear to be strongly dependent on the material (or the class of material) under investigation and cannot be expected to be more generally applicable (Ref 5).

*In a SP test, displacement is normally measured by means of an extensometer or LVDT (linear voltage displacement transducer), which records either the relative movement of the punch with respect to the lower die (punch displacement, u) or the deflection of the central portion of the disk on the opposite side of the punch (specimen deflection, v).

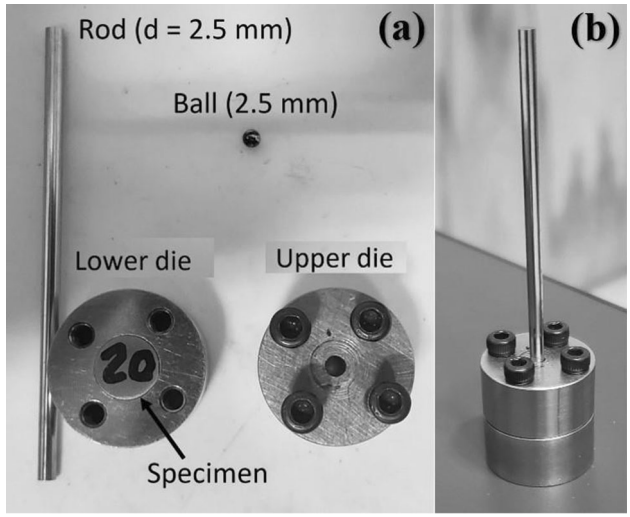

Fig. 2 SP testing fixture used at NIST, shown disassembled (a) and assembled (b)

2. Experimental Setup

The fixture developed at NIST for testing SP specimens consists of an upper and a lower die, a rod (100 mm long, 2.5 mm diameter), and a ball (2.5 mm diameter). The combination of the rod and ball constitute the punch, which is driven through the specimen, encapsulated between the upper and lower die. The fixture is shown in Fig. 2 in both disassembled (a) and assembled (b) form.

The fixture was mounted on a universal electro-mechanical test machine, equipped with a 5 kN capacity load cell and an extensometer. The extensometer was attached to one of the columns of the machine in order to measure the relative displacement between the machine actuator and the machine frame, in close proximity to the punch. Figure 3 shows the fixture mounted on the test machine and the positioning of the extensometer with respect to the machine actuator.

All tests were performed at room temperature (21 °C ± 2 °C) in actuator displacement control, at rates between 0.001 mm/s and 0.003 mm/s. Force, actuator displacement, and punch displacement (extensometer) data were recorded at a sampling frequency of 1 Hz. To account for the compliance of the test system on punch displacement, actuator and extensometer displacements were recorded without a specimen in place, and then subtracted from displacements measured during the tests. Data analysis was conducted by means of spreadsheet-based software developed in-house, in accordance with the provisions of the recently published ASTM E3205-20 (Ref 6), which was developed by the ASTM E10.02 subcommittee on *Behavior and Use of Nuclear Materials*.

3. Material and Testing Matrix

This investigation was performed on additively manufactured Ti-6Al-4V. Additive manufacturing (AM), also known as 3D printing, is a process in which material is joined or solidified under computer control to create a three-dimensional object, with material being added together (such as liquid molecules or powder grains being fused together), typically

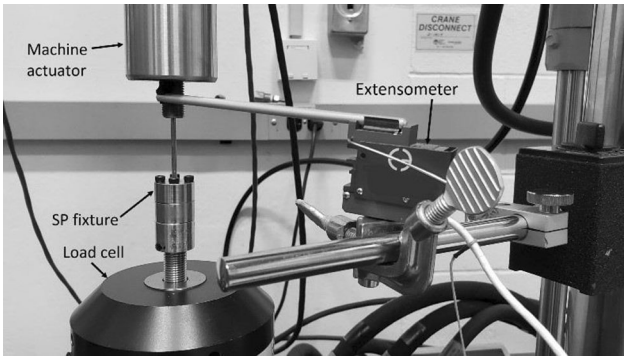

Fig. 3 SP testing fixture mounted on the test machine with the extensometer for punch displacement measurement

layer by layer (Ref 7). In the 1990s, 3D printing was considered only suitable for producing functional or aesthetical prototypes. Nowadays, the precision, repeatability, and material range have increased to the point where AM is considered to be an industrial production technology.

The sale of AM products and services was projected to exceed US$6.5 billion worldwide by 2019 (Ref 8). To enable use of metal AM in applications where fatigue and fracture can occur, a recent NIST/ASTM workshop (Ref 9) identified the need for a deeper understanding of fatigue and fracture behavior of these materials through detailed investigations of processing–structure–property–performance relationships. Although AM Ti-6Al-4V processing–structure–property relationships have been previously extensively studied (Ref 10, 11), the current literature lacks sufficient small punch measurements and detailed analysis of correlations to relevant mechanical properties. It is the goal of this study to assess the suitability of this technique for AM metals. If successful, the small punch test method, through its small sample size, may aid in establishment of highly desired rapid qualification techniques for metal AM.

Ti-6Al-4V (commonly, and hereinafter, called Ti64) is the most widely used titanium alloy, featuring good machinability and excellent mechanical properties (Ref 12). It offers the best all-round performance for a variety of weight-reduction applications in aerospace, automotive, and marine equipment. Its high strength, low weight, and outstanding corrosion resistance have led to a wide range of successful applications that demand high levels of reliable performance in surgery and medicine (e.g., implants and prosthesis), aerospace, automotive, chemical plants, power generation, oil and gas extraction, sports, and other major industries.

3.1 AM Processing Parameters

In this investigation, SP tests were performed on AM Ti64 disks in order to assess the technique's capability of yielding reliable estimates of the material's tensile and fracture toughness properties.

The material was fabricated using an EBM powder bed fusion Arcam** A1 machine (software version 3.2.132,60 kV, 50 µm layer thickness) and standard Arcam Ti-6Al-4V gas-atomized powder (70 µm average diameter). The powder composition conforms to ASTM F2924-14 (Ref 13). Chemical analysis of manufactured parts (including any effects resulting from HIP treatments) were previously measured (Ref 14).

**Certain commercial software, equipment, instruments, or materials are identified in this paper to adequately specify the experimental procedure. Such identification is not intended to imply recommendation or endorsement by the National Institute of Standards and Technology, nor is it intended to imply that the equipment or materials identified are necessarily the best available for the purpose.

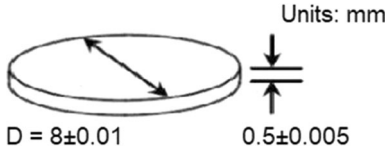

Fig. 4 Dimensions and tolerances of the SP specimens

The following conditions (AM processing parameters), for which conventional tensile and fracture toughness test results had been previously measured, were investigated (Ref 15, 16)†:

a. As-built condition (without heat treatment).
b. Non-standard Ti64 HIP (800 °C, 100 MPa, 2 h, Ar environment, standard 12 °C/minute heating and cooling rates).
c. Standard Ti64 HIP (900 °C, 100 MPa, 2 h, Ar environment, standard 12 °C/minute heating and cooling rates).
d. Non-standard Ti64 HIP (1050 °C, 100 MPa, 2 h, rapid 1600 °C/minute cooling in Ar) with an additional HIP (800 °C, 30 MPa, 2 h, slow 12 °C/minute cooling in Ar-meant for martensite tempering).
e. Scan lengths of:

e1. 78 mm and
e2. 26 mm.

3.2 Machining and Surface Finish

All SP disks were machined from AM Ti64 non-supported blocks (*i.e.*, directly attached to the build plate) by electro-discharge machining (EDM) in accordance with the drawing in Fig. 4.

The relationship between the orientation of tensile, small punch, and fracture toughness specimens is illustrated in Fig. 5. Z is the build direction.

After machining, some of the specimens were polished to the surface finish required by ASTM 3205-20 (Ref 6), Ra $\leq$ 0.25 µm, by means of abrasive paper with an abrasive grit size designation P400 followed by fine grinding (P1200). As a result, polished disks had a thickness ranging from 0.43 mm to 0.48 mm. The rest of the specimens (EDM "rough" disks) had surface roughness in the range Ra = 3 µm to 4 µm. This allowed us to investigate the influence of surface finish on SP test results.

3.3 SP Tests Performed

Overall, 55 SP disks (36 rough and 19 polished) were tested, according to the test matrix shown in Table 1.

The main tensile properties for the different conditions, obtained from conventional tensile tests (Ref 14) and used for the correlations with SP test results, are listed in Table 2.

†Scan length is a manufacturer-specific parameter that corresponds to the distance the electron beam travels on a single track before turning around to begin the next track. It has been shown to determine energy density and affect texture (Ref 16).

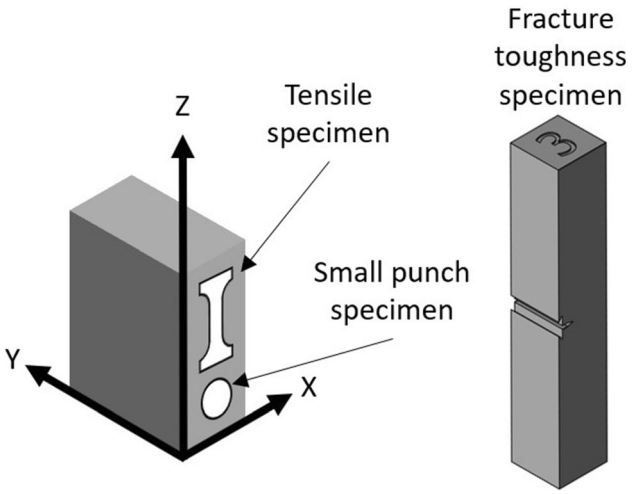

Fig. 5 Orientation of tensile, small punch, and fracture toughness specimens for AM Ti64, with respect to the build direction (Z)

Table 1 Test matrix (for material conditions, see Sect. 3.1)

	Number of tests performed	
Material condition	**Rough disks**	**Polished disks**
a,e1	6	3
a,e2	6	3
b,e1	6	4
c,e1	6	2
c,e2	6	4
d,e1	6	3

Table 2 Tensile properties (average values and standard deviations) for the different material conditions (Ref 14).

Material condition	R_{p02}, MPa	R_m, MPa	ε_u, %	ε_f, %
a,e1	879±4.2	981±5.3	9.5±0.4	27.8±2.8
a,e2	875±7.4	972±5.4	9.1±0.5	25.5±2.6
b,e1	864±6.4	969±6.1	10.1±0.8	31.7±0.9
c,e1	838±6.1	951±4.8	10.0±0.5	31.0±1.1
c,e2	799±15.3	918±9.7	10.0±1.0	31.8±2.6
d,e1	885±6.2	985±11.7	7.9±0.9	18.8±2.6

4. Microstructural Investigations

Representative backscattered electron (BSE) images of the microstructures were acquired with a field-emission scanning electron microscope (20 kV) and are shown in Fig. 6. The microstructure of each material condition is composed of dark α-Ti laths and bright β-Ti ribs. Approximately 120 measurements from multiple images were used to evaluate the grain size of each material condition. The α-Ti lath thickness of the as-built condition is 1.16-0.26 µm (Fig. 6a). When subjected to HIP treatments at temperatures below the β-transus (980 °C), the morphology of the laths remains unchanged, but the 900 °C HIP treatment coarsens the lath thickness to 2.17-0.51 µm, whereas the lath thickness of the 800 °C HIP treatment condition only coarsens to 1.45-0.40 µm. When comparing the as-built condition (Fig. 6a) to the HIP treatment conducted above the β-transus (Fig. 6d), the aspect ratio of α-Ti laths increases (the laths become longer, indicating recrystallization), but the lath thickness of condition d (1.20-0.32 µm) is not statistically different than the as-built condition. While images of both scan lengths are not shown, the effect of scan length on α-Ti lath thickness and on the morphology of the elongated prior-β grains is negligible. Regarding anisotropy in the microstructure, our previous work (Ref 15, 16) provides detailed discussion on changes in crystallographic texture and prior-β grain morphology (elongated in the build direction) that stem from changes in EBM scan length and HIP parameters. Finally, it should be noted that no porosity was detected in conditions b, c, and d (the HIP treatments), based on x-ray computed tomography measurements with a resolution of 3 µm × 3 µm × 3 µm.

5. SP Test Results

An example of force/punch displacement curve for AM Ti64 (condition b,e1) is shown in Fig. 7. Depending on material condition, one or more force drops were observed before, at, and/or after maximum force.

The curves obtained here are qualitatively very similar to those reported in the literature for other investigations on electron beam melted (EBM) AM Ti64 (Ref 17, 18) and differ significantly from conventional SP test records for steel specimens, as in the example illustrated in Fig. 1. However, the five regions shown in Fig. 1 can still be identified, see Fig. 7, and the analysis of the test can be conducted in accordance with (Ref 6).

Tables 3 and 4 summarize average values and relative standard deviations, respectively, for the main characteristic values of force, punch displacement, and energy obtained for the different conditions. Note that average values in Table 3 should not be compared directly between rough and polished specimens, as these latter had a lower thickness (0.43 mm-0.47 mm) than the former (0.5 mm). Relative standard deviations in Table 4, however, can be legitimately compared.

The SP parameter that exhibits the least variability (1.3%-3.3%) is the maximum force F_m, whereas the elastic–plastic transition force F_e, which is calculated from the intersection of two linear fits (Ref 6), yielded relative standard deviations in the range 2.4%-15.0%. Interestingly, displacements at maximum force, u_m, generally showed larger scatter than displacements corresponding to a 20% force drop from the maximum, u_f. In terms of calculated energies, the most consistent parameter is the fracture energy, E_{SP}.

No obvious effect of surface finish (rough vs. polished) could be detected on the variability of SP parameters.

6. Correlations with Tensile Properties

Many empirical correlations between normalized SP parameters and conventional tensile properties have been proposed in the literature, almost exclusively for steels. For most of these correlations, the accuracy of the predicted strength values (yield

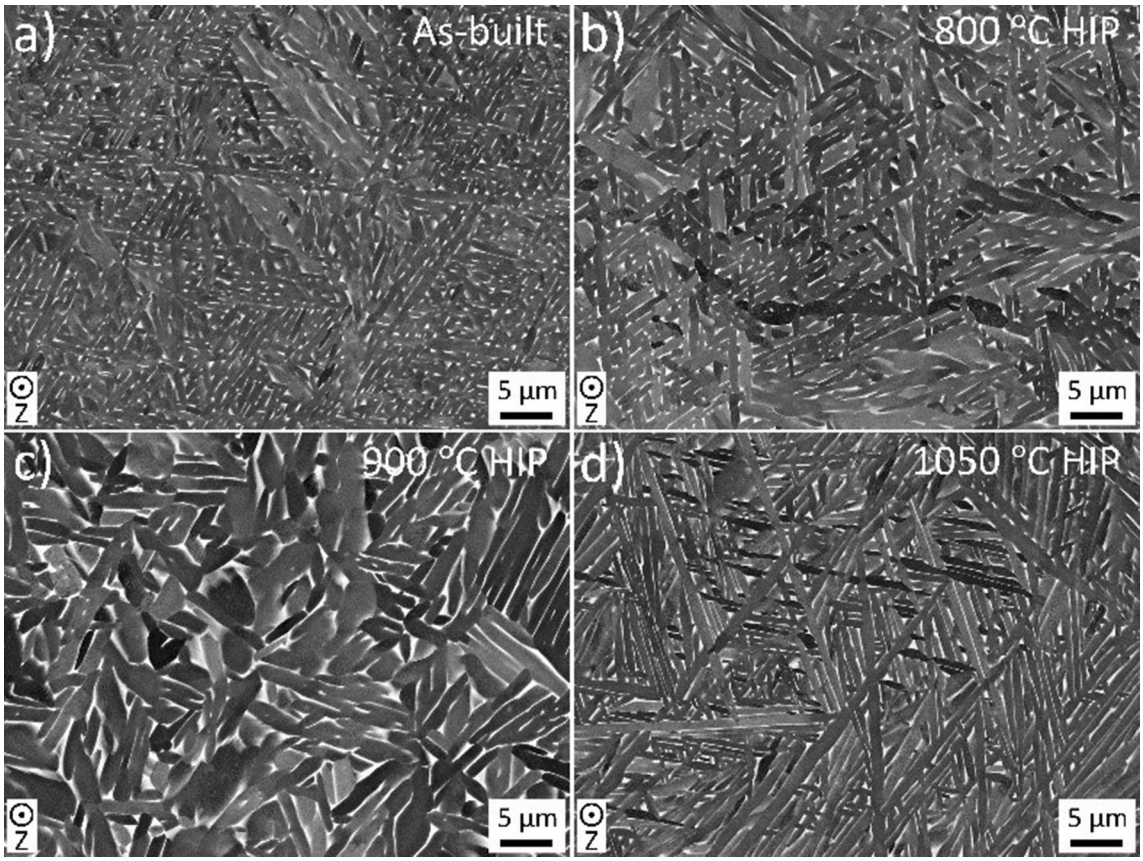

Fig. 6 Backscattered electron images recorded for the following material conditions: (a) as-built, (b) non-standard Ti64 HIP treatment of 800 °C, (c) standard Ti64 HIP treatment of 900 °C, and (d) non-standard Ti64 dual HIP treatment of 1050 °C and 800 °C. All parts in this figure were manufactured with the same scan length (78 mm) and Z indicates the orientation of the image with respect to the build direction (see Fig. 1)

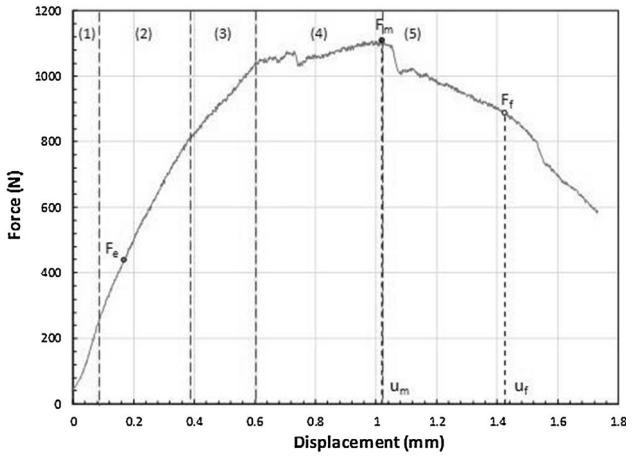

Fig. 7 Force-punch displacement curve for a SP test on AM Ti64 (as-built, scan length = 78 mm)

and ultimate) can be reported to be in the order of ± 25 MPa. Specifically:

- Yield strength has been mostly correlated with $F_e/\ h_0^2$ (Ref 19-25). Alternative correlations for R_{p02} have been proposed with:

  $F_{h0/10,off}$, normalized by h_0^2 (Ref 21);
  $F_{0.1mm,off}$, normalized by h_0^2 (Ref 20, 22);
  F_{ept}, normalized by h_0^2 (Ref 25);
  $F_{e1.5}$, normalized by h_0^2 (Ref 25);
  $Slope_{ini}$, normalized by h_0 (Ref 26).

- Tensile strength has been mostly correlated with F_m, normalized either by h_0^2 (Ref 21, 23, 25) or $h_0 u_m$ (Ref 19-25, 27). Other force values that have been correlated with R_m are:

  F_{infl}, normalized by $h_0 \cdot u_m$ (Ref 25);
  $F_{0.48mm}$ (Ref 27), $F_{0.645mm}$ (Ref 25), and $F_{0.65mm}$ (Ref 28), all normalized by h_0^2.

- Total elongation has been correlated with u_m (Ref 21, 29), u_m/h_0 (Ref 21, 29), and $\frac{u_f - h_0}{h_0}$ (Ref 31).

Almost every correlation is of the generic linear form:

$$Y = \alpha_1 X + \alpha_2, \qquad \text{(Eq 1)}$$

where Y is the tensile property of interest, X is the normalized SP parameter, and α_1, α_2 are slope and intercept, respectively, of the least-squares linear regression between X and Y.

Table 3 Main characteristic values of force, displacement, and energy (average values) obtained from SP tests on AM Ti64

Material condition	Specimen condition	F_e, N	F_m, N	u_m, mm	u_f, mm	E_{SP}, J	E_m, J	E_{PL}, J
a,e1	Rough	433	1084	0.928	1.387	1.16	0.71	0.49
	Polished	410	981	0.910	1.291	1.01	0.66	0.51
a,e2	Rough	408	1102	1.098	1.501	1.21	0.80	0.47
	Polished	403	968.7	0.780	1.232	0.93	0.53	0.38
b,e1	Rough	452	1103	0.985	1.431	1.14	0.69	0.36
	Polished	389	986	0.782	1.366	1.06	0.54	0.39
c,e1	Rough	385	1084	1.018	1.499	1.16	0.68	0.32
	Polished	386	1057	0.923	1.377	1.13	0.69	0.50
c,e2	Rough	382	1088	1.112	1.709	1.38	0.78	0.43
	Polished	404	1018	0.728	1.340	1.06	0.49	0.31
d,e1	Rough	417	119	1.039	1.513	1.28	0.76	0.39
	Polished	411	1080	0.706	1.176	0.96	0.49	0.31

Table 4 Relative standard deviations for the main characteristic values of force, displacement, and energy obtained from SP tests on AM Ti64

Material condition	Specimen condition	N	s_{Fe}, %	s_{Fm}, %	s_{um}, %	s_{uf}, %	s_{ESP}, %	s_{Em}, %	s_{EPL}, %
a,e1	Rough	6	15.0	2.3	6.7	4.6	7.4	10.5	17.0
	Polished	3	9.1	2.9	6.5	4.1	2.6	5.5	5.3
a,e2	Rough	6	8.7	2.7	6.0	4.6	5.5	9.8	18.7
	Polished	3	8.6	1.3	11.3	1.1	2.2	15.1	21.8
b,e1	Rough	6	5.0	3.2	11.2	5.1	7.8	17.1	34.6
	Polished	4	8.8	2.3	16.4	6.6	5.1	24.8	35.3
c,e1	Rough	6	11.1	3.3	16.0	7.2	9.0	16.0	54.7
	Polished	2	10.3	3.3	4.9	7.3	7.0	5.6	7.7
c,e2	Rough	6	6.9	2.1	12.6	6.6	7.6	19.3	36.0
	Polished	4	10.7	3.1	33.2	1.7	3.2	47.4	69.1
d,e1	Rough	6	10.3	2.2	3.1	5.0	6.5	5.7	14.1
	Polished	3	2.4	2.1	2.6	8.0	9.3	3.8	7.4

6.1 Yield Strength Correlations

The strongest correlations[‡] were found between R_{p02} and F_e/h_0^2 (Fig. 8), $r = 0.67$ for rough specimens and $r = 0.85$ for polished specimens:[§,§§]

$$R_{p02} = 0.1462\frac{F_e}{h_0^2} + 610.82(\text{rough}) \quad \text{(Eq 2)}$$

$$R_{p02} = 0.4042\frac{F_e}{h_0^2} + 60.785(\text{polished}) \quad \text{(Eq 3)}$$

Strong empirical correlations were also found between R_{p02} and $F_{h0/10,off}/h_0^2$ for rough specimens ($r = 0.69$) and $F_{0.1mm}/h_0^2$ for polished specimens ($r = 0.77$):[§§,§§]

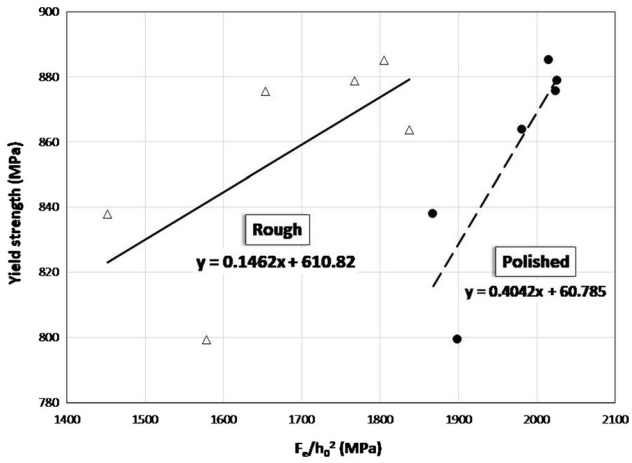

Fig. 8 Empirical correlations between R_{p02} and $\frac{F_e}{h_0^2}$ for rough and polished SP specimens

$$R_{p02} = 0.1853\frac{F_{h0/10,off}}{h_0^2} + 372.04(\text{rough}) \quad \text{(Eq 4)}$$

$$R_{p02} = 0.3204\frac{F_{0.1mm,off}}{h_0^2} - 239.58(\text{polished}) \quad \text{(Eq 5)}$$

[‡]The strength of the correlations is hereinafter defined based on the value of Pearson correlation coefficient, r: strong ($r > 0.70$), moderate ($0.70 \le r < 0.5$), weak ($0.50 \le r < 0.30$), or absent/no correlation ($r \le 0.30$).
[§]Standard errors of the fit coefficients: 0.0818 (slope) and 138.13 (intercept).
[§§]Standard errors of the fit coefficients: 0.1228 (slope) and 242.006 (intercept).
[§§]Standard errors of the fit coefficients: 0.0960 (slope) and 251.20 (intercept).
[§§]Standard errors of the fit coefficients: 0.1336 (slope) and 457.13 (intercept).

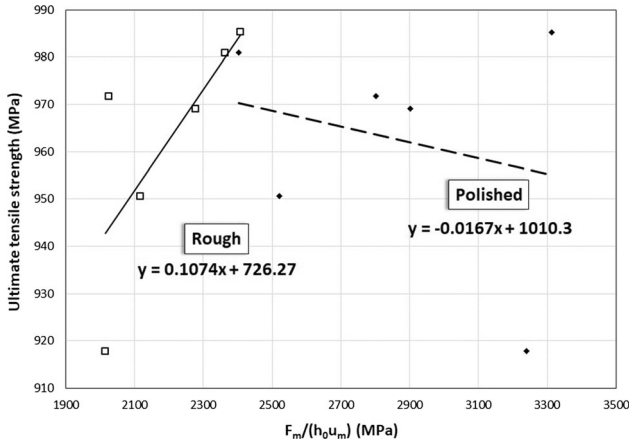

Fig. 9 Empirical correlations between R_m and $\frac{F_m}{h_0 u_m}$ for rough and polished SP specimens

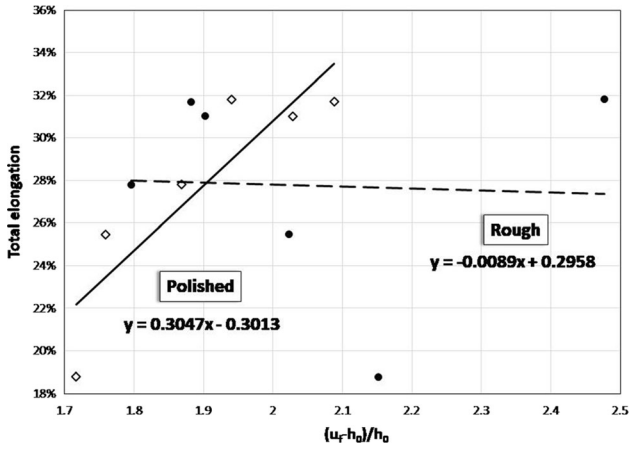

Fig. 10 Empirical correlations between ε_t and $\frac{u_f - h_0}{h_0}$ for rough and polished SP specimens

Additional correlations attempted were moderate, weak, or nonexistent.

6.2 Tensile Strength Correlations

The quality of the empirical correlations established between tensile strength and SP parameters was generally poor.

For rough specimens, the strongest correlation was found between R_m and $F_m/(h_0 u_m)$ (r = 0.74, Fig. 9). Strong/moderate correlations with R_m were also established with $F_{0.65mm}/\ h_0^2$ (r = 0.73) and $F_{0.48mm}/\ h_0^2$ (r = 0.70).

For polished specimens, the only acceptable (moderate) correlation was between R_m and $F_{0.48mm}/\ h_0^2$ (r = 0.51). All other correlations were found to be nonexistent ($r \leq 0.30$).

The best correlations for the two types of specimens were found to have the following expressions:[§§,§§]

$$R_m = 0.1074 \frac{F_m}{h_0 u_m} + 726.27 (\text{rough}) \quad \text{(Eq 6)}$$

$$R_m = 0.1362 \frac{F_{0.48mm}}{h_0^2} + 374.43 (\text{polished}) \quad \text{(Eq 7)}$$

6.3 Elongation Correlations

For rough specimens, negative (and therefore non-physical) correlations were found between ε_t and both u_m/h_0 (r = -0.27) and $\frac{u_f - h_0}{h_0}$ (r = -0.04, Fig. 10). In the case of polished specimens, however, both correlations were positive, and the correlation with $\frac{u_f - h_0}{h_0}$ (Fig. 10) was quite strong (r = 0.88):[§§]

$$\varepsilon_t = 0.3047 \frac{u_f - h_0}{h_0} - 0.3013 (\text{polished}). \quad \text{(Eq 8)}$$

We also attempted to correlate uniform elongation, ε_u, to the normalized punch displacement at maximum force, u_m/h_0 (Fig. 11). Once again, a non-physical negative relationship was found for rough specimens, whereas a weak (r = 0.30) positive correlation was obtained for polished specimens.

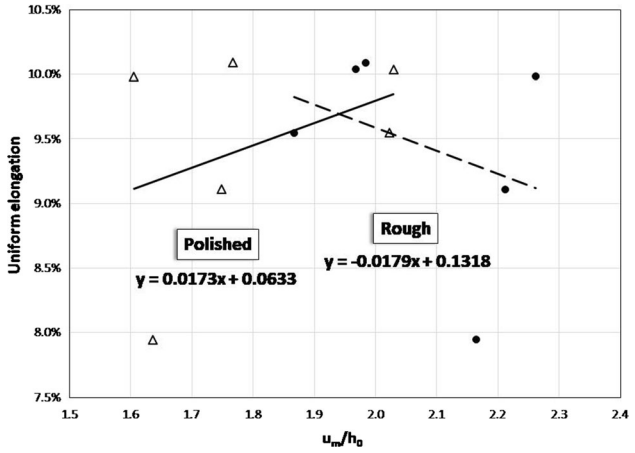

Fig. 11 Empirical correlations between ε_u and $\frac{u_m}{h_0}$ for rough and polished SP specimens

6.4 Fractography

Prior to sectioning of the fractured small punch specimens, secondary electron (SE) images were recorded from multiple fracture surfaces, shown in Fig. 12. Fractography investigations revealed microvoid coalescence in all material conditions (confirmed with multiple specimens). Generally speaking, the macroscopic features observed on fracture surfaces of condition d (the HIP treatment conducted above the β-transus, including a rapid quench) were more faceted.

7. Correlations with Fracture Toughness

In the literature, fracture toughness has been often estimated from SP test results by means of analytical approaches involving finite element calculations (Ref 32, 33). Most of the published empirical correlations were established between

[§§]Standard errors of the fit coefficients: 0.0490 (slope) and 108.11 (intercept).
[§§]Standard errors of the fit coefficients: 0.1138 (slope) and 491.47 (intercept).
[§§]Standard errors of the fit coefficients: 0.0806 (slope) and 0.1536 (intercept).

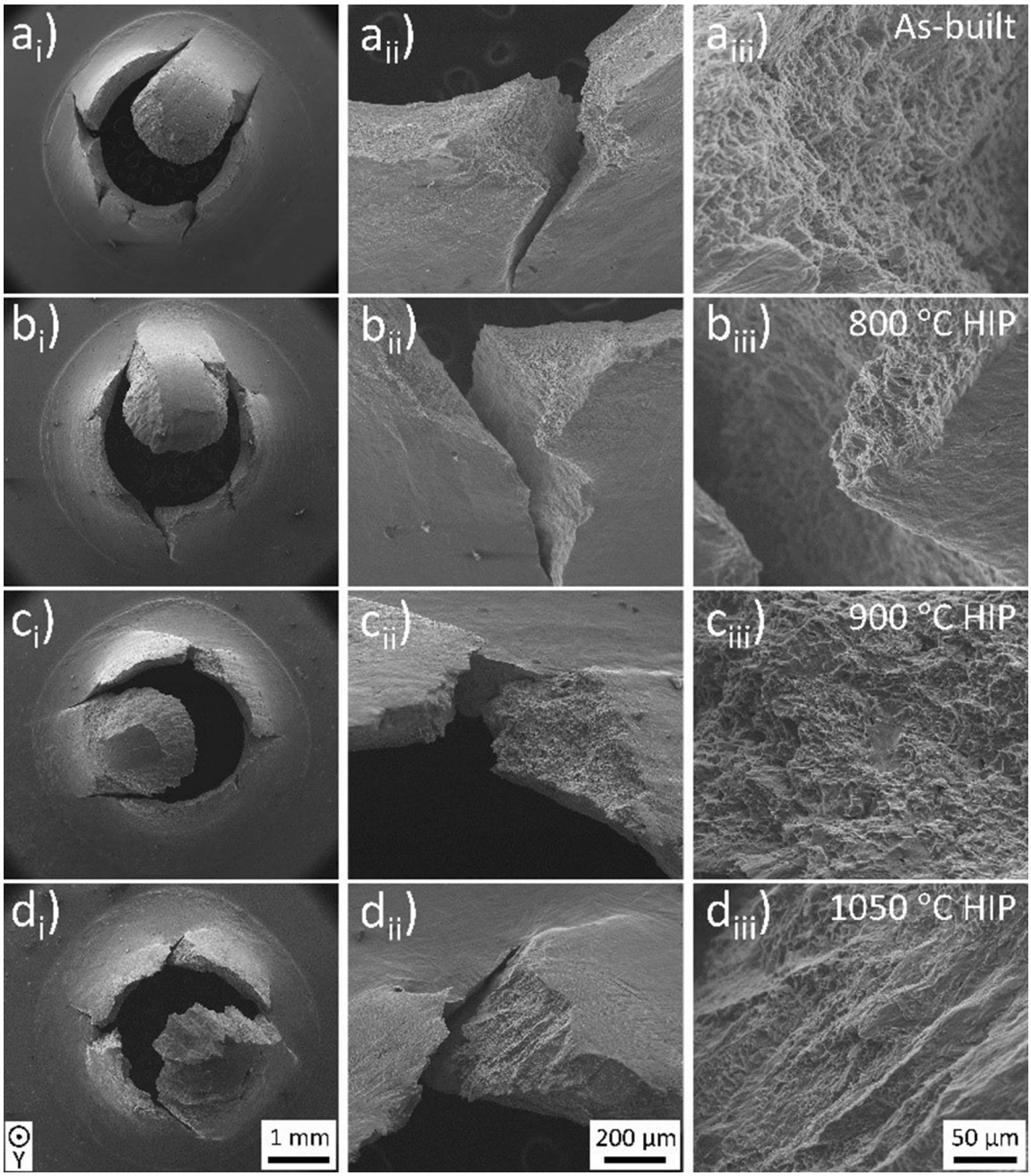

Fig. 12 Secondary electron images (20 kV) recorded at different magnifications (indicated by i, ii, and iii) for the following material conditions: (a) as-built, (b) non-standard Ti64 HIP treatment of 800 °C, (c) standard Ti64 HIP treatment of 900 °C, and (d) non-standard Ti64 dual HIP treatment of 1050 °C and 800 °C. All parts in this figure were manufactured with the same scan length (78 mm) and Y indicates the orientation of the sample with respect to the build direction (see Fig. 1)

critical J-integral (J_{Ic}, J_Q) and effective (or biaxial) fracture strain, ε_f. This is generally calculated as (Ref 21, 34-36):

$$\varepsilon_f = ln\left(\frac{h_0}{h_f}\right). \quad \text{(Eq 9)}$$

For the investigated material, the room temperature elastic–plastic fracture toughness had been measured in four conditions (as-built and 900 °C HIP, two scan lengths) on fatigue pre-cracked Charpy-type specimens during a previous investigation (Ref 37, 38). The size-sensitive critical value of J-integral, J_Q, was determined by means of the elastic compliance single-specimen methodology (Table 5).

For the same four AM Ti64 conditions, measurements of initial and final minimum thickness were taken on 2-3 tested SP specimens per condition and surface finish (rough and polished). Secondary electron images were acquired with a scanning electron microscope (SEM). Thickness measurements were acquired via SE imaging of vertically cross-sectioned specimens mounted such that the cross-sectional thickness was perpendicular to the electron beam. Due to the specific morphology of the investigated material in the fracture region, these measurements were found to be subject to significant uncertainties, as seen in Fig. 13, which compares a sample from AM Ti64 to a sample from a pressure vessel steel (A533B Cl.

Table 5 Elastic–plastic fracture toughness (average values and standard deviations) measured on four AM Ti64 material conditions (Ref 37, 38)

Material condition	J_Q, kN/m^2
a,e1	121.14 ± 14.80
a,e2	93.23 ± 6.63
c,e1	157.67 ± 20.73
c,e2	151.61 ± 19.57

Table 6 Effective fracture strains (average values and standard deviations) measured on four AM Ti64 material conditions

Material condition	ε_f
a,e1	0.103 ± 0.038
a,e2	0.121 ± 0.035
c,e1	0.174 ± 0.032
c,e2	0.171 ± 0.048

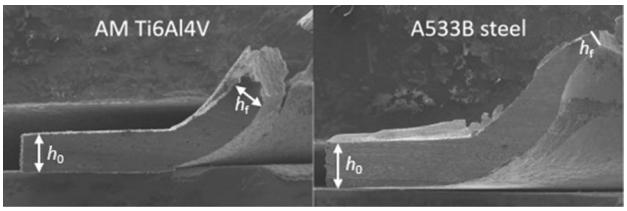

Fig. 13 Measurements of initial and final (minimum) thickness on SP specimens of AM Ti64 (left) A533B Cl.1 steel (right)

1). Identifying the minimum thickness h_f appears more straightforward for the steel sample (right side of the figure) than for the AM Ti64 sample (left side).

Therefore, all thickness measurements were independently performed by three of the authors, and average values were used to derive fracture toughness estimates for the investigated conditions by means of Eq 9. Individual measurements by the three authors had standard deviations lower than 10%. A simple t test showed no statistical difference between rough and polished specimens; hence, overall mean values of initial and final thickness were used to obtain the values of fracture strain shown in Table 6 for the different conditions.

Using the data in Tables 5 and 6, the following empirical relationship was obtained:[§§]

$$J_Q = 683.57\varepsilon_f + 33.49, \qquad \text{(Eq 10)}$$

corresponding to a strong degree of correlation (r = 0.82). As shown in Fig. 14 the comparison between Eq 10 and similar correlations obtained on steels (Ref 35, 39) clearly shows that, at the same level of toughness, AM Ti64 undergoes significantly less deformation at fracture than steel.

In this study, we also investigated novel correlations between J_Q and the following normalized SP energy values: $\frac{E_{SP}}{h_0 u_f}$, $\frac{E_m}{h_0 u_m}$, and $\frac{E_{PL}}{h_0 u_{m,pl}}$. In each case, SP energy was normalized by the product of the initial thickness by the corresponding displacement value. For E_{PL}, the plastic component of u_m was calculated as:

$$u_{m,pl} = u_m - \frac{F_m}{\text{Slope}_{ini}}. \qquad \text{(Eq 11)}$$

[§§]Standard errors of the fit coefficients: 333.15 (slope) and 48.60 (intercept).

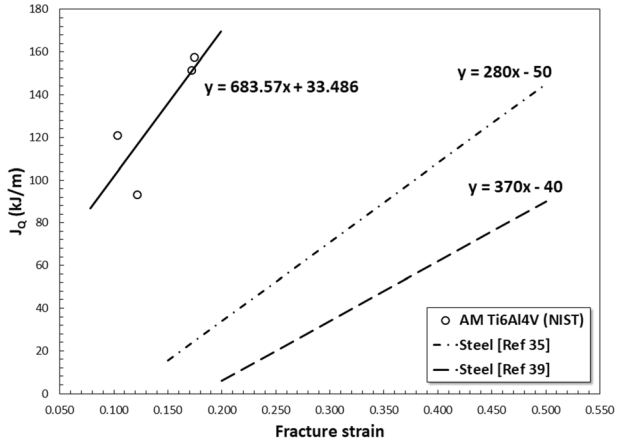

Fig. 14 Relationship between fracture strain and critical toughness for AM Ti64 (this study) and steel (Ref 35, 39)

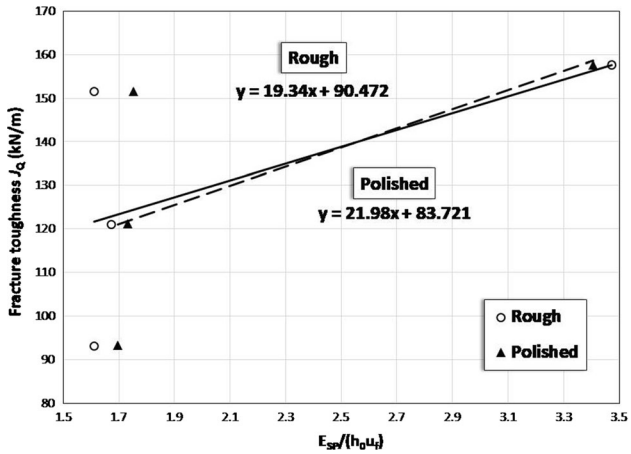

Fig. 15 Empirical correlations between J_Q and $\frac{u_m}{h_0}$ for rough and polished SP specimens

For both rough and polished specimens, moderate correlations were found between J_Q and the normalized fracture energy $\frac{E_{SP}}{h_0 u_f}$ (r = 0.60 and 0.62, respectively-Fig. 15). The remaining correlations were negative and therefore unacceptable for rough specimens, while in the case of polished specimens a weak correlation was obtained for the plastic energy, $\frac{E_{PL}}{h_0 u_{m,pl}}$ (r = 0.43), and no correlation was observed with the normalized total energy, $\frac{E_m}{h_0 u_m}$ (r = 0.18). It's also interesting to note in Fig. 15 that the effect of surface finish on normalized fracture energy appears negligible.

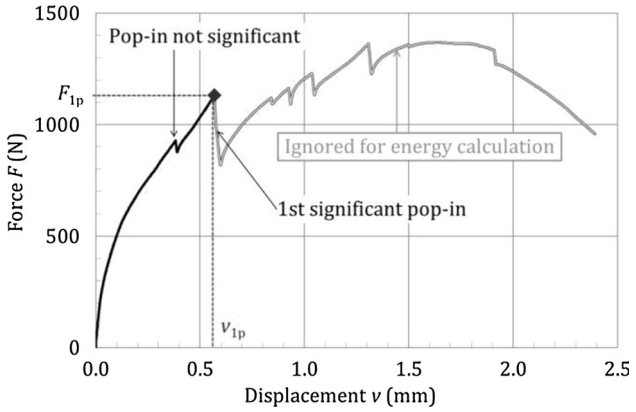

Fig. 16 Force–displacement curve for a SP test on ODS 14YWT steel (Ref 40)

8. Discussion

Across the board, the quality of empirical correlations between mechanical properties and SP parameters for AM Ti64 was found to be worse than for steels as reported in the open literature. This is hardly surprising, considering that the small punch methodology was developed for application to high-quality (very homogeneous and "clean") materials in the power industry (Ref 1) and was found to be inaccurate for highly anisotropic materials, such as oxide–dispersion–strengthened (ODS) steels (Ref 40). As an example, the force–displacement curve for a SP test on ODS 14YWT steel (Ref 40) shown in Fig. 16 exhibits several force drops ("pop-in" type events), associated with the steel's susceptibility to secondary cracking and has a different form than the classical SP curve for homogeneous steels (Fig. 1). Moreover, a recent study (Ref 41) investigating the SP method (validated with finite element models) determined that the SP method is suitable for evaluating tensile properties of materials that exhibit isotropic plastic responses.

It should also be noted that the range of tensile properties for the AM Ti64 investigated conditions, with respect to the property average value, was relatively limited, particularly in the case of R_{p02} and R_m (10.1% and 7%, respectively). This makes it even more difficult to obtain strong correlations, particularly in the presence of significant experimental variability. When comparing only the effects of HIP parameters, the differences in small punch measurements of strength in the AM Ti64 specimens followed a general Hall–Petch effect where an increase in strength was likely caused by a decrease in lath thickness.

As far as the influence of specimen surface finish is concerned, we can generally state that polished specimens correlate better with AM Ti64 tensile properties than rough specimens, which supports the inclusion of the Ra $<$ 0.25 µm requirement in both ASTM E3205 (Ref 6) and the CEN Workshop Agreement CWA15627:2007 (Ref 34). Moreover, we observe that normalized force values are systematically larger for polished specimens, see Figs 8 and 9. This implies that surface roughness also affects the mechanical behavior of the specimen in terms of both large-scale yielding and fracture. In terms of specimen failure, it is suspected that crack initiation at the specimen surface can occur more easily (*i.e.*, at lower stresses) in the case of rough specimens.

9. Conclusions

The overall quality of the empirical correlations that we obtained between tensile/fracture properties and SP test parameters for six conditions of AM Ti64 is not very satisfactory. Several correlations were found to be nonexistent or weak at best. This is not an unexpected conclusion, since the small punch methodology has been shown to have limited applicability for highly anisotropic materials, such as those produced via additive manufacturing.

The strongest correlations (correlation coefficient $r > 0.70$) were found between:

- Yield strength (R_{p02}) and normalized SP elastic–plastic transition force (F_e/h_0^2), Eq 2 and 3.
- Yield strength (R_{p02}) and normalized SP force at $h_0/10$ offset ($F_{h0,off}/h_0^2$) for rough specimens (Ra $>$ 3 µm), Eq 4.
- Yield strength (R_{p02}) and normalized SP force at 0.1 mm offset ($F_{0.1mm,off}/h_0^2$) for polished specimens (Ra $<$ 0.25 µm), Eq 5.
- Total elongation (ε_t) and normalized SP displacement at fracture $\left(\frac{u_f - h_0}{h_0}\right)$ for polished specimens, Eq 8.
- Fracture toughness (J_Q) and effective fracture strain (ε_f), Eq 10.

The influence of surface roughness on SP characteristic parameters was found to be significant on specimen yielding and fracture, in that these phenomena tend to occur earlier in the test in the case of rougher specimens. Across the board, polished specimens (Ra $<$ 0.25 µm, in accordance with current normative or pre-normative documents) appear to yield better correlations. Finally, it was demonstrated that HIP parameter selection causes measurable differences in strengths measured during small punch testing.

Acknowledgments

We wish to express sincere gratitude to Ross Rentz, who contributed significantly to the development and realization of the small punch test methodology and equipment at NIST.

References

1. E. Lucon, Testing of Small-Sized Specimens, Comprehensive Materials Processing, C. J. Van Tyne, ed., 2014, Elsevier Ltd., Vol. 1, p 135–163. https://doi.org/10.1016/B978-0-08-096532-1.00110-2
2. O. K. Harling, M. Lee, D.-S. Sohn, G. Kohse, and C.W. Lau, The MIT Miniaturised Disc Bend Test, The Use of Small-Scale Specimens for Testing Irradiated Material, ASTM STP 888, W. R. Corwin and G. E. Lucas, eds., 1986, ASTM, Philadelphia, PA, p 50–65
3. M. P. Manahan, A. E. Browning, A. S. Argon, and O. K. Harling, Miniaturised Disc Bend Test Technique Development and Application, The Use of Small-Scale Specimens for Testing Irradiated Material, ASTM STP 888, W. R. Corwin and G. E. Lucas, eds., 1986, ASTM, Philadelphia, PA, p 17–49
4. G.L. Hankin, M.B. Toloczko, M.L. Hamilton, F.A. Garner and R.G. Faulkner, Validation of the Shear Punch–Tensile Correlation Technique Using Irradiated Materials, *J. Nucl. Mater.*, 1998, **258–263**, p 1651–1656. https://doi.org/10.1016/S0022-3115(98)00203-7
5. V. Bicego, E. Lucon, and C. Sampietri, The 'Small Punch' Technique for Evaluating Quasi Non-Destructively the Mechanical Properties of Steels, Fracture from Defects, ECF 12: Proceedings of the Twelfth

European Conference on Fracture, M. W. Brown, E. R. de los Rios, K. J. Miller, eds., 1998, EMAS Publishing, London, Vol. 1, p 1273–1278
6. Standard Test Method for Small Punch Testing of Metallic Materials, E3205-20, Annual Book of ASTM Standards, Part 03.01, ASTM International, 2020
7. I. Gibson, D. Rosen and B. Stucker, *Additive Manufacturing Technologies*, Springer, New York, 2015. https://doi.org/10.1007/978-1-4939-2113-3
8. M. Gorelik, Additive Manufacturing in the Context of Structural Integrity, *Int. J. Fatigue*, 2017, **94**, p 168–177. https://doi.org/10.1016/j.ijfatigue.2016.07.005
9. N. Hrabe, N. Barbosa, S.R. Daniewicz, and N. Shamsaei, Findings from the NIST/ASTM Workshop on Mechanical Behavior of Additive Manufacturing Components, NIST Technical Note 1936, Boulder, CO, 2016. https://doi.org/10.6028/NIST.TN.1936
10. X. Tan, K. Yihong, J.Y. Tan, M. Descoins, D. Mangelinck, S.B. Tor, K.F. Leong and C.K. Chua, Graded Microstructure and Mechanical Properties of Additive Manufactured Ti-6Al-4V Via Electron Beam Melting, *Acta Mater.*, 2015, **97**, p 1–16. https://doi.org/10.1016/j.actamat.2015.06.036
11. X. Zhao, S. Li, M. Zhang, Y. Liu, T.B. Sercombe, S. Wang, Y. Hao, R. Yang and L.E. Murr, Comparison of the Microstructures and Mechanical Properties of Ti-6Al-4V Fabricated by Selective Laser Melting and Electron Beam Melting, *Mater. Des.*, 2016, **95**, p 21–31. https://doi.org/10.1016/j.matdes.2015.12.135
12. V. Tuninetti, Mechanical Behavior of Ti-6Al-4V Titanium Alloy, Editorial Académica Española, 2018
13. Standard Specification for Additive Manufacturing Titanium-6 Aluminum-4 Vanadium with Powder Bed Fusion, F2924-14, Annual Book of ASTM Standards, Part 10.04, ASTM International, 2020
14. J. Benzing, N. Hrabe, T. Quinn, R. White, R. Rentz and M. Ahlfors, Hot Isostatic Pressing (HIP) to Achieve Isotropic Microstructure and Retain as-Built Strength in an Additive Manufacturing Titanium Alloy (Ti-6Al-4V), *Mater. Lett.*, 2019, **257**, p 126690. https://doi.org/10.1016/j.matlet.2019.126690
15. N. Hrabe, R. White and E. Lucon, Effects of Internal Porosity and Crystallographic Texture on Charpy Absorbed Energy of Electron Beam Melting Titanium Alloy (Ti-6Al-4V), *Mater. Sci. Eng. A*, 2019, **742**, p 269–277. https://doi.org/10.1016/j.msea.2018.11.005
16. N. Hrabe, T. Gnäupel-Herold and T. Quinn, Fatigue Properties of a Titanium Alloy (Ti-6Al-4V) Fabricated Via Electron Beam Melting (EBM): Effects of Internal Defects and Residual Stress, *Int. J. Fatigue*, 2017, **94**, p 200–210. https://doi.org/10.1016/j.ijfatigue.2016.04.022
17. R. Lancaster, G. Davies, H. Illsley, S. Jeffs and G. Baxter, Structural Integrity of an Electron Beam Melted Titanium, *Materials*, 2016, **9**, p 470. https://doi.org/10.3390/ma9060470
18. H. Illsley, R. Lancaster, R. Hurst, S. Jeffs and G. Baxter, Mechanical Property Characterisation of Electron Beam Melted (EBM) via Small Punch Tensile Testing, *Key Eng. Mater.*, 2017, **734**, p 51–60
19. Y. Ruan, P. Spätig and M. Victoria, Assessment of Mechanical Properties of the Martensitic Steel EUROFER97 by Means of Punch Tests, *J. Nucl. Mat.*, 2002, **307–311**, p 236–239. https://doi.org/10.1016/S0022-3115(02)01194-7
20. K. Matocha, Determination of actual tensile and fracture characteristics of critical components of industrial plants under long term operation by SPT, in ASME 2012 Pressure Vessels & Piping Conference, PVP2012, Toronto, Canada, July 15-19, 2012, ASME Paper No. PVP2012-78553. https://doi.org/10.1115/PVP2012-78553
21. T.E. García, C. Rodríguez, F.J. Belzunce and C. Suárez, Estimation of the Mechanical Properties of Metallic Materials by Means of the Small Punch Test, *J. Alloys Compd.*, 2014, **582**, p 708–717. https://doi.org/10.1016/j.jallcom.2013.08.009
22. K. Matocha, Small-Punch Testing for Tensile and Fracture Behavior: Experiences and Way Forward, Small Specimen Test Techniques: 6th Volume, ASTM STP 1576, M.A. Sokolov and E. Lucon, eds., ASTM International, West Conshohocken, PA, 2015, p 145–159. https://doi.org/10.1520/STP157620140005
23. M. Bruchhausen, S. Holmström, I. Simonovski, T. Austin, J.-M. Lapetite, J.-M. Ripplinger and de F. Haan, , Recent Developments in Small Punch Testing: Tensile Properties and DBTT, *Theor. Appl. Fract. Mech.*, 2016, **86**, p 2–10. https://doi.org/10.1016/j.tafmec.2016.09.012
24. E. Altstadt, H.E. Ge, V. Kuksenko, M. Serrano, M. Houska, M. Lasan, M. Bruchhausen, M. Lapetite and Y. Dai, Critical Evaluation of the Small Punch Test as a Screening Procedure for Mechanical Properties, *J. Nucl. Mater.*, 2016, **472**, p 186–195. https://doi.org/10.1016/j.jnucmat.2015.07.029
25. A. Janča, J. Siegl and P. Haušild, Small Punch Test Evaluation Methods for Material Characterization, *J. Nucl. Mater.*, 2016, **481**, p 201–213. https://doi.org/10.1016/j.jnucmat.2016.09.015
26. J.C. Chica, P.M.B. Díez, and M.P. Calzada, Development of an improved correlation method for the yield strength of steel alloys in the small punch test, in 5th International Small Sample Test Techniques Conference, SSTT2018, Swansea University, UK, July 10-12, 2018, Ubiquity Proceedings, 2018. https://doi.org/10.5334/uproc.12
27. K. Kumar, A. Pooleery, K. Madhusoodanan, R.N. Singh, J.K. Chakravartty, R.S. Shriwastaw, B.K. Dutta and R.K. Sinha, Evaluation of Ultimate Tensile Strength Using Miniature Disk Bend Test, *J. Nucl. Mater.*, 2015, **461**, p 100–111. https://doi.org/10.1016/j.jnucmat.2015.02.029
28. E. Altstadt, M. Houska, I. Simonovski, M. Bruchhausen, S. Holmström and R. Lacalle, On the Estimation of Ultimate Tensile Stress from Small Punch Testing, *Int. J. Mech. Sci.*, 2018, **136**, p 85–93. https://doi.org/10.1016/j.ijmecsci.2017.12.016
29. E. Fleury and J.S. Ha, On the Estimation of Ultimate Tensile Stress from Small Punch Testing, *Int. J. Pressure Vessel Piping*, 1998, **75**, p 699–706
30. C. Rodriguez, J.G. Cabezas, E. Cardenas, F.J. Belzunce and C. Betegon, Mechanical Properties Characterization of Heat-Affected Zone Using the Small Punch Test, *Weld. Res.*, 2009, **88**, p 188–192
31. S. Yang, X. Ling and D. Peng, Elastic and Plastic Deformation Behavior Analysis in Small Punch Test for Mechanical Properties Evaluation, *J. Central South Univ.*, 2018, **25**(4), p 747–753. https://doi.org/10.1007/s11771-018-3779-7
32. J.R. Foulds, and C.W. Jewett, Miniature Specimen Test Technique for Estimating Toughness, Report GS-7526, Electric Power Research Institute, Palo Alto, CA, 1991
33. J.R. Foulds, M. Wu, S. Srivastav, and C.W. Jewett, Fracture and Tensile Properties of ASTM Cross-Comparison Exercise A533B Steel by Small Punch Testing, Small Specimen Test Techniques, ASTM STP 1329, W.R. Corwin, S.T. Rosinski, and E. Van Walle, eds., ASTM, Philadelphia, PA, 1997, p 557–574
34. Small Punch Test Method for Metallic Materials, CEN Workshop Agreement, CWA 15627:2007, European Committee for Standardization, Brussels, Belgium, 2007
35. Z.-X. Wang, H.-J. Shi, J. Lu, P. Shi and X.-F. Ma, Small Punch Testing for Assessing the Fracture Properties of the Reactor Vessel Steel with Different Thicknesses, *Nucl. Eng. Des.*, 2008, **238**, p 3186–3193. https://doi.org/10.1016/j.nucengdes.2008.07.013
36. R.C. Hurst and K. Matocha, A Renaissance in the Use of the Small Punch Testing Technique, Transactions, SMiRT-23, Manchester, UK, August 10–14, 2015, *Division II*, 2015 https://doi.org/10.1115/PVP2015-45095
37. E. Lucon, J. Benzing and N. Hrabe, "Room Temperature Fracture Toughness Characterization of Additively Manufactured Ti-6Al-4V", NIST Technical Note 2065, Boulder, *Colorado*, 2019 https://doi.org/10.6028/NIST.TN.2065
38. E. Lucon, J. Benzing and N. Hrabe, Effect of Precrack Configuration and Lack-of-Fusion on the Elastic-Plastic Fracture Toughness of Additively Manufactured Ti-6Al-4V parts, *Mater. Perform. Charact.*, 2020, **9**(5), p 701–713. https://doi.org/10.1520/MPC20190155
39. X. Mao, M. Saito and H. Takahashi, Small Punch Test to Predict Ductile Fracture Toughness J_{IC} and Brittle Fracture Toughness K_{IC}, *Scr. Metall. Mater.*, 1991, **25**(11), p 2481–2485. https://doi.org/10.1016/0956-716X(91)90053-4
40. E. Altstadt, M. Houska and A. Das, Effect of Anisotropic Microstructure of ODS Steels on Small Punch Test Results, *Theor. Appl. Fract. Mech.*, 2019, **100**, p 191–199. https://doi.org/10.1016/j.tafmec.2019.01.014
41. N. Leclerc, A. Khosravani, S. Hashemi, D.B. Miracle and S.R. Kalidindi, Correlation of Measured Load-Displacement Curves in Small Punch Tests with Tensile Stress-Strain Curves, *Acta Mat.*, 2021, **204**, p 116501. https://doi.org/10.1016/j.actamat.2020.116501